

Characterization of Alumina Porous Nano Structure With Adjusting Fuel Ratio Via Modified Auto Combustion Method

M. Ghasemifard, M. Ghamari*, E. Fathi, A. R. Karbalaei, and M. Iziy
Nano Technology Laboratory, Engineering department,
Esfarayen University of Technology, esfarayen, Iran, 98195-96619

Abstract— Nano-alumina particles (Al_2O_3 -NPs) was prepared via modified auto-combustion method (MACM) using optimum ratio of citric and nitric acid as fuel. Al_2O_3 -NPs were annealed at 750°C, 900°C and 1200°C for 2h. Effect of salt molar weight to fuel (SMW/F) on structure was investigated by X-ray diffraction (XRD). The XRD results revealed that the samples produced at 900°C and 1200°C were crystalline with a cubic and rhombohedral structure, respectively. In order to figure out the particle aggregation state, nano-particles size distribution and porosity surface, transmission electron microscopy (TEM), dynamic light scattering (DLS) and BET analysis technique were investigated, respectively. The results show that SMW/F=2.1 can be used as an optimum ratio for polymerization and stabilizer in ACM.

Keywords—Auto-combustion, Nano-alumina porous, Dynamic light scattering.

I. INTRODUCTION

γ - Al_2O_3 -NPs is classified as porous materials. Porous materials have many extraordinary properties concerning porosity, microstructures and mechanical strength [1]. The porous materials are used in many industrial areas because of their novel properties due to their wide applications, such as catalyst carriers, catalytic support for many chemical reactions [2-5]. The properties of porous Al_2O_3 have been developed by various routes such as precipitation[6], hydrothermal [7], sol-gel [8], freeze casting [9, 10], gelcasting [11, 12], ice templating [13, 14] and combustion synthesis [15]. However, find an efficient way is a challenge to prepare powders with particle size in about several nanometers. Therefore, we made an attempt to prepare Al_2O_3 -NPs by a novel wet chemical method namely, MACM. Simple experimental setup, narrow distribution of nano-particles, high-purity, homogeneous and potential large-scale production are advantages of MACM [16]. The influence of stability constant of metal citrates in MACM on the combustion process is more effective than metal ions,

which are able to give electrons to the fuel by changing their oxidation state like Al. On the other hand, although the non-redox metal ions can form metal citrates as well, the poor effect has been reported on Lead and Barium[17, 18]. The rate of calcination is another important parameter in this process. In this project, a combination of citric and nitric acid was used as fuel. The effect of pH on particle size and particle size distribution (PSD) as a function of calcination and molar weight was investigated. All of samples were characterized by X-ray diffraction (XRD), transmission electron microscopy (TEM), dynamic light scattering (DLS) and BET analysis.

II. EXPERIMENTAL PROCEDURE

Samples were synthesized using aluminum nitrate [$\text{Al}(\text{NO}_3)_3$, 99% purity] and citric acid ($\text{C}_6\text{H}_8\text{O}_7$, 99% purity) as starting materials, which were obtained from Merck and nitric acid (HNO_3 , 99% purity) was obtained by Fluka, Switzerland. Aqueous solution of single cation (i.e. Al^{3+}) was prepared by dissolving salt's precursor (15g) in distilled water (35ml). The solutions were added to the aqueous solution of citric acid under continuous stirring at 55-65°C and finally at the end the pH of the sol was maintained at 5.5 using ammonium hydroxide. At low pH, citric acid decomposes at 171°C. This behavior is described by the fact that the metal cations and the citric acid do not form any complex with each other. In this study after the sol was heated at about 80°C, in order to obtain the peroxy-citrato-nitrate gel, solution is prepared at pH=5.5 and in 135°C. The color of gel transforms into brownish after that the auto-combustion occurs when the temperature increased to 280°C. After gel was combusted, the resultant samples were calcined at 750°C, 900°C and 1200°C. More details regarding the synthesis process are described elsewhere[17]. The calcination rate was 4°C/min. At desired temperature samples were kept for 2h. Samples were characterized by X-ray diffraction (XRD), (spinning sample rate: 0.02deg./s) in the ranges (20-80deg), transmission electron microscopy (TEM), dynamic light scattering (DLS) and BET analysis.

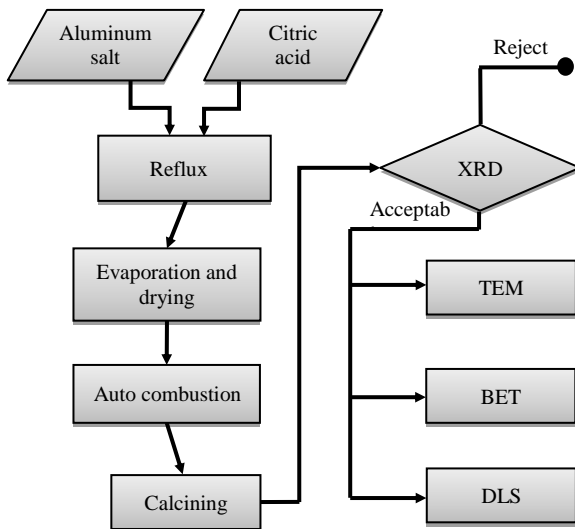


Fig.1. Flow diagram for Al_2O_3 nano-powder preparation procedure.

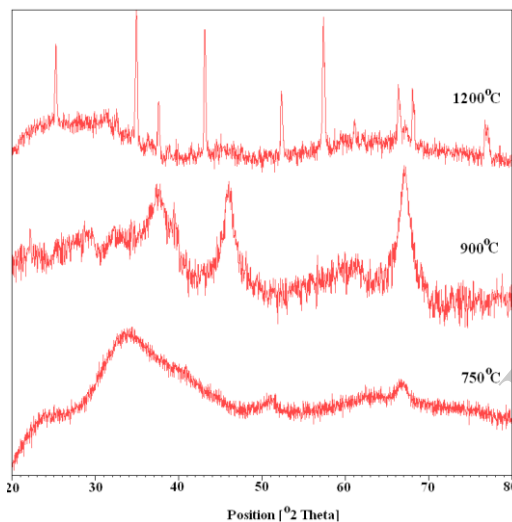


Fig. 2. XRD patterns of Al_2O_3 nano-powders calcined at different temperatures.

III. Results and discussion

A. XRD Measurements

The phase formation and orientation of Al_2O_3 nano-powder were investigated using X-ray diffraction (spinning sample rate: 0.02deg./s) in the ranges (20-80deg). X-ray diffraction patterns of nano-powders with $\text{CuK}\alpha_1$ at different temperatures are shown in figure 2.

The diffraction patterns have been analyzed using the X'pert package. It was found that the presence of $\gamma\text{-Al}_2\text{O}_3$ (cubic phase) at temperatures below 900°C can be identified from figure 2. The XRD results also reveal the existence of rhombohedra phase as alpha-alumina ($\alpha\text{-Al}_2\text{O}_3$) in 1200°C. On the other hand, for cubic phase (110), (111) and (211) peaks and the (113), (104), (012) and (116) peaks were used for rhombohedra phase analysis. The lattice constants were found to be $a=b=0.475\text{nm}$ and $c=1.299\text{nm}$. The structural results for nano alumina in this work and the values obtained

by the others are summarized in Table I.

TABLE I. The structural results of nano alumina

Temperature (°C)	2Theta (°)	hkl	Structure	Lattice parameter (Å)
900	37.85	110	cubic	a=4.132
	45.67	111		
	66.87	211		
1200	43.36	113	rhomboheda	a=b=4.758 c=12.991
	35.14	104		
	57.52	116		
[19]T.C.=1200°C	43.36	113	rhomboheda	a=b=4.7588 c=12.992
37.78	104			
57.52	116			
[20]T.C.=750°C	45.73	111	cubic	a=7.914

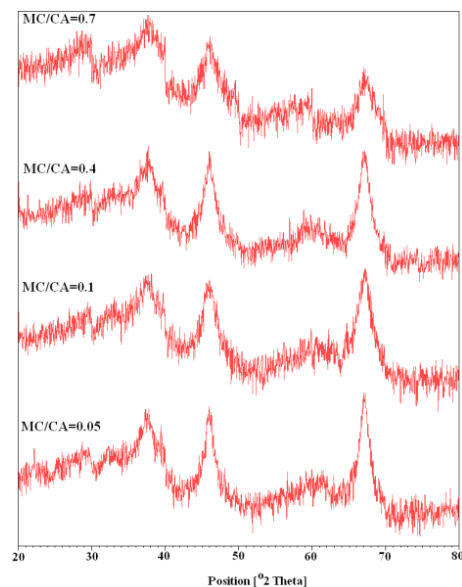


Fig. 3. XRD patterns of Al_2O_3 nano-powders at different MC/CA ratio.

XRD patterns of different nano-powders with different MC/CA ratio are shown in figure 3.

As can be seen from figure 3 gamma-alumina ($\gamma\text{-Al}_2\text{O}_3$) exists in all samples. From figure 3 and using Scherrer equation it can be estimated that there is a gradual increase in the crystallite size when the MC/CA ratio decreases. The mean crystallite size grew by 27nm from MC/CA=0.05 to MC/CA=0.7.

B. Effect of Fuel Molar Ratio

In a same ratio of citric acid to nitric acid the quality of combustion reaction of mono-elements depends on the molar weight. The trend of the maximum combustion intensity is observed at different CA/NA ratio. On the other hand, lower intensity of the auto-combustion reaction occurs at higher CA/NA ratios. This result observed in electroceramics as well, and it is in good agreement with the results of Ghasemifard and et al. [21]. Formation of the ligand electrons with the metal in the solution is one of factors which increases stability of the metal-citrate complex and decreases the power of fuel. The crystallite size of Al_2O_3 -NPs has been determined as a

function of CA/NA ratios using the Scherrer equation:

$$D = k\lambda / \beta \cos\theta \quad (1)$$

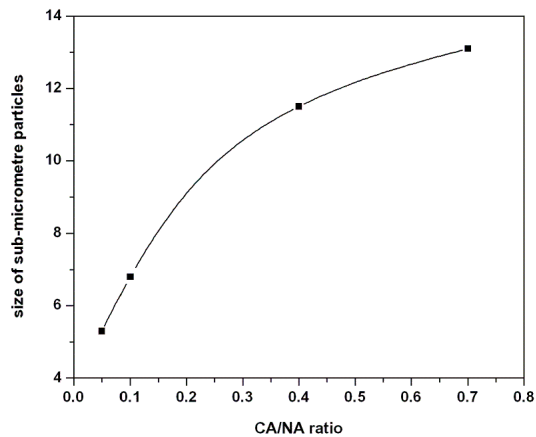


Fig. 4. The crystallite size as a function of CA/NA ratio for nano-alumina.

where D is the crystallite size, λ is the wavelength of the CuK α radiation, k is a constant equal to unity, β is corrected peak width at half maximum intensity and θ is peak position (45.67° used for all lines). Crystallite size of Al₂O₃-NPs increases, as CA/NA ratios increase. Crystallite size of Al₂O₃-NPs as function of CA/NA ratio is shown in figure 4. From figure 4 it can be estimated that the crystallite size rose steeply at first then continued its upward movement more slowly towards the end of the CA/NA ratio.

The combustion process is highly affected by the molar weight of elements. The auto combustion mechanisms were evidenced are depending on the SMW/F ratio. From the results observed that when SMW/F ratio decreases from 0.7 to 0.05, the intensity of the combustion process increased.

This mechanism favors the synthesis nano-oxide powder with high molar mass.

C. Nanoscale Characterizations

Using TEM, particle size and morphology were evaluated. Typical TEM image of Al₂O₃-NPs, heat treated at 900°C for two hours, prepared by the auto-combustion method are shown in figure 5. From TEM analysis, the primary particle size of the nano powders can be determined. It can be seen from the figure 5 that there are three types of particles with different geometries, figure 5 (a) polyhedral shaped particles with average particle size below 34nm, figure 5 (b) spherical particles with average size below 55nm and figure 5 (c) porous mass with pore average size below 10nm. According to figure 5 (c), the porosities of the porous Al₂O₃ nano-powder are about 7.5nm. γ -Al₂O₃-NPs is classified as porous materials[22].

From figure 6 inhomogeneous nano-porous structure of alumina is clearly shown, as revealed by the right part of the picture. The nano-porous in figure 6 is represented by the white holes with a diameter of nanometers. The particles size distribution of nano-alumina was measured based on the Dynamic Light Scattering (DLS) method using a particle size analyzer (Malvern Instrument Ltd., Malvern, England). The size of particles and agglomerates or aggregation state of the nano-particles can be determined by dynamic light scattered (DLS)[23-25]. DLS which are made on poly-dispersed of different sized particles and the histogram of the particle size distribution from TEM images calcined at 900°C, are presented in figure 7.

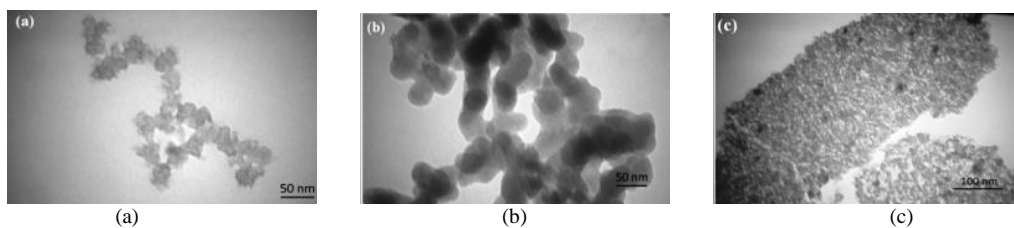


Fig. 5. TEM image of Al₂O₃-NPs obtained at 900°C (a) polyhedral shaped particles, (b) spherical particles and (c) porous particles.

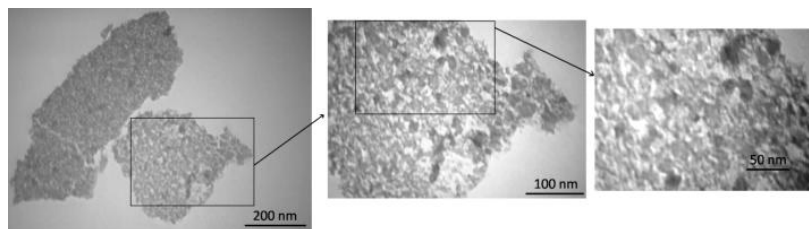


Fig. 6. TEM images of nano-porous γ -alumina.

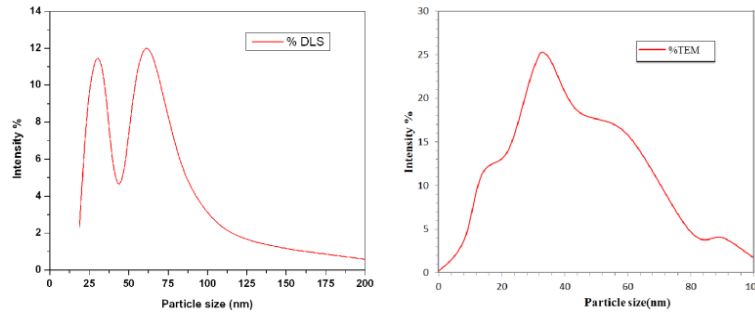


Fig. 7. Size distribution from TEM and DLS measurements of nano- Al_2O_3

TABLE II. The size distribution results of nano γ -alumina

Peak	% Number width (nm)		% Volume width (nm)		% Intensity width (nm)	
Peak1	49.2	7.38	43.3	27.71	74.6	76.74
Peak2	50.8	45.81	19.3	432.2	13.7	377.8
Peak3	-	-	22.9	8.27	8.6	8.184

In a non-agglomerated colloidal solution, the measured diameter of DLS will be similar (if the particle shape be spherical) or steadily larger than the TEM size [26, 27]. In comparison with TEM particle size the DLS measurement have a large variability in the particle size if the nano-particles are agglomerated. As can be seen from figure 7 the maximum distribution of particle size of γ -alumina powder by DLS is 49.2% for 30.88nm and 50.8% for 78.48nm, while for TEM average diameter is 46nm. The size distribution results of nano γ -alumina in this work and the values obtained by the others are summarized in Table 2.

From Table 2 it can be seen that the maximum size distribution of nano γ -alumina by number at first peak (diam.=30.88nm) is confirmed by volume at (diam.=170.4nm). In fact, the size distribution of nano-alumina by volume was quantized as the relative intensity of particles. The pore size distribution or specific surface area of nano-alumina can be evaluated by BET (Brunauer -Emmett -Teller) analysis [28, 29]. The specific surface area is strongly dependent on degree of calcination temperature. The pore average size and specific surface area of γ -alumina is less than 7.5nm and $146\text{m}^2\text{g}^{-1}$, respectively.

IV. CONCLUSION

Al_2O_3 -NPs were synthesized by modified auto-combustion method. The effect of metal cations (MC) to citric acid (CA) ratio and citric acid (CA) to nitric acid (NA) ratio on the structure of powders were investigated with XRD, TEM, DLS and BET. The results show that the structure of powders is significantly influenced by the molar ratio of citric acid to metal cations and vice versa for the molar ratio of citric to nitric acid. The combustion rate decreases with increasing MC/CA ratio. The crystallite size of the as-formed oxide powders increases with increasing the MC/CA. The crystalline phases transform from cubic to rhombohedra with increasing calcination temperature from 900°C to 1200°C . The mean pore

size was found to be around 7.5nm for the samples prepared by the auto combustion method. The results show that ratio of fuels, type of fuel and pH of the solution are three main factors influencing the process. Comparing DLS and TEM, because γ - Al_2O_3 nano-particles are agglomerated in DLS the measured diameter is larger than the real size (TEM). DLS and BET analysis show that γ -alumina with a larger surface area is due to greater number of smaller pore size.

ACKNOWLEDGMENT

The authors gratefully acknowledge the financial support by Esfarayen University of Technology Khorasan Shomali Province, Iran (Grant No: 92.706.63).

REFERENCES

- [1] K. Ishizaki, S. Komarneni, M. Nanko, Porous Materials, Process Technology and Applications, London: Kluwer academic publishers, pp. 181-198, 1998.
- [2] R. H. Perry, Chemical Engineers Handbook. 6st ed. New York: McGraw-Hill, pp. 23,1984.
- [3] J. Tikkanen, K. A. Gross, C. C. Berndt, V. Pitkanen, J. Keskinen, S. Raghun, M. Rajala, J. Karthikeyan, "Characteristics of the liquid flame spray process," Surf Coat Technol, 90, pp. 210-216, 1997.
- [4] M. I. F. Macedo, C. C. Osawa, C. A. Bertran, "Sol-gel synthesis of transparent alumina gel and pure gamma alumina by urea hydrolysis of aluminum nitrate," Journal of sol-gel science and technology, 30(3), pp. 135-140, 2004.
- [5] K. Ada, Y. Sarikaya, T. Alemdaroglu, M. Onal, "Thermal behaviour of alumina precursor obtained by the aluminium sulphate-urea reaction in boiling aqueous solution," Ceramics International, 29(5): pp. 513-518, 2003.
- [6] P. K. Shrama, V. V. Varadan, V. K. Varadan, J. Europ. Ceram. Soc., 23, pp. 659, 2003.
- [7] M. Zhangy, L. Y. Hu, J. C. Han, Z. H. Jiang, Ceram. int, 36, 2010.
- [8] A. Kritikaki, A. Tsetsekou, "Fabrication of porous alumina ceramics from powder mixtures with sol-gel derived nanometer alumina: Effect of mixing method," Journal of the European ceramic Society, 29(9): pp. 1603-1611, 2009.
- [9] L. Jing, K. H. Zuo, F. Q. Zhang, X. Chun, Y. F. Fu, D. L. Jiang, Y. P. Zeng, Ceram int, 36, 2010.
- [10] K. Lu, C. S. Kessler, and R. M. Davis, "Optimization of a nanoparticle suspension for freeze casting," Journal of the American Ceramic Society, 89(8): pp. 2459-2465, 2006.
- [11] M. Takahashi, R. L. Menchavez, M. Fuji, takegami h "Opportunities of porous ceramics fabricated by gelcasting in mitigating environmental issues," Journal of the European ceramic Society, 29(5): pp. 823-828, 2009.

- [12] F. S. Ortega, P. Sepulveda, V. C. Pandolfelli, "Monomer systems for the gelcasting of foams," *Journal of the European ceramic Society*, 22(9): pp. 1395-1401, 2002.
- [13] H. Nishihara, S. R. Mukai, Y. Fujii, T. Tago, T. Masuda, H. Tamon, "Preparation of monolithic $\text{SiO}_2\text{-Al}_2\text{O}_3$ cryogels with inter-connected macropores through ice templating," *J. Mater. Chem.*, 16(31), pp. 3231-3236, 2006.
- [14] G. Liu, "Porous $\text{Al}_2\text{O}_3\text{-ZrO}_2$ composites fabricated by an ice template method," *Scripta Materialia*, 62(7), pp. 466-468, 2010.
- [15] M. Ghasemifard, S. Hosseini, G.H. Khorrami, "Synthesis and structure of PMN-PT ceramic nanopowder free from pyrochlore phase," *Ceramics International*, 35(7), pp. 2899-2905, 2009.
- [16] M. Ghasemifard, S. M. Hoeseini, A. Khorsand Zak, Gh.H. Khorrami, "Microstructural and optical characterization of PZT nanopowder prepared at low temperature," *Physica E*, 41, pp. 418-422, 2009.
- [17] M. Ghasemifard, S. M. Hosseini, M. M. Mohaghheghi Bagheri, N. Shahtahmasbi, "Microstructure comparison of PMN-PT and PMN-PZT prepared by gel-combustion method at optimized temperature," *Physica E*, 41, pp. 1701-1706, 2009.
- [18] M. Ghasemifard, "OPTICAL PROPERTIES OF BMN-BT FERROELECTRIC THIN FILMS PREPARED BY SPRAY PYROLYSIS DEPOSITION," *Modern Physics Letters B*, 26(02), 2012.
- [19] F. R. Feret, D. Roy, C. Boulanger, "Determination of alpha and beta alumina in ceramic alumina by X-ray diffraction," *Spectrochimica Acta Part B*, 55, pp. 1051-1061, 2000.
- [20] B. O'Connor, D. Li, B. K. Gan, B. Latella, J. Carter, "Time-resolved Studies of Alumina Ceramics Processing with Neutron and Synchrotron Radiation Data," in *DENVER X-RAY CONFERENCE*, pp. 659-667, 1997.
- [21] M. Ghasemifard, "Dielectric, piezoelectric and electrical study of 0.65PMN-0.20PZT-0.15PT relaxor ceramic," *Eur. Phys. J. Appl. Phys.*, 54, 2011.
- [22] H. L. Jiang, Qiang "Recent progress in synergistic catalysis over heterometallic nanoparticles," *J. Mater Chem*, 21, pp. 13705-13725, 2011.
- [23] B. Akbari, M. P. Tavandashti, M. Zandrahimi, "PARTICLE SIZE CHARACTERIZATION OF NANOPARTICLES - A PRACTICAL APPROACH," *Iranian Journal of Materials Science & Engineering*, 8(2), pp. 48-56, 2011.
- [24] P. Bowen, "Particle size distribution measurement from millimeters to nanometers and from rods to platelets," *Journal of dispersion science and technology*, 23(5), pp. 631-662, 2002.
- [25] A. F. Rawle, "Micron sized nano-materials," *Powder technology*, 174(1), pp. 6-9, 2007.
- [26] M. Staiger, P. Bowen, J. Ketterer, J. Bohonek, "Particle size distribution measurement and assessment of agglomeration of commercial nanosized ceramic particles," *Journal of dispersion science and technology*, 23(5), pp. 619-630, 2002.
- [27] R. M. German, "A Measure of the Number of Particles in Agglomerates," *International journal of powder metallurgy*, 32(4), pp. 365-373, 1996.
- [28] S. Brunauer, P. H. Emmett, E. Teller, "The determination of pore volume and area distributions in porous substances. I. Computations from nitrogen isotherms," *Journal of the American Chemical Society*, 73, pp. 373-380, 1951.
- [29] E. P. Barrett, L.G. Joyner, P. P. Halenda, "The determination of pore volume and area distributions in porous substances. I. Computations from nitrogen isotherms," *Journal of the American Chemical Society*, 73(1), pp. 373-380, 1951.